




^{119}Sn Mössbauer spectroscopy in the study of metamagnetic shape memory alloys

I. Unzueta^{1,3}  · J. López-García² · V. Sánchez-Alarcos^{5,6} ·
V. Recarte^{5,6} · J. I. Pérez-Landazábal^{5,6} ·
J. A. Rodríguez-Velamazán² · J. S. Garitaonandia^{3,4} ·
J. A. García^{3,4} · F. Plazaola¹

Published online: 15 August 2018
© Springer Nature Switzerland AG 2018

Abstract

The effect of combined mechanical and thermal treatments in the magnetostructural properties is studied in a Ni-Mn-Sn metamagnetic shape memory alloy, by X-ray diffraction, powder neutron diffraction, calorimetry, magnetometry and ^{119}Sn Mössbauer spectroscopy. A $\text{Ni}_{50}\text{Mn}_{35}\text{Sn}_{15}$ alloy has been mechanically milled and then annealed at different temperatures in order to produce different microstructural states. The milling and the post-annealing processes do not produce any variation of transition temperatures and atomic order. However, the induced microstructural distortions affect greatly the martensitic transformation. Milling promotes antiferromagnetic coupling between Mn atoms, resulting in a significant decrease in the saturation magnetization that recovers with annealing. Moreover, the temperature width of the transformation is considerably affected by the mechanically induced local strain. Last but not least, the recovery of the microstructural distortions induced by milling is directly related to the intensity of the non-magnetic component revealed by ^{119}Sn Mössbauer spectroscopy. This result opens the possibility of quantifying the whole contribution of defects and local strain on the martensitic transformation in Ni-Mn-Sn alloys.

Keywords Heusler alloys · Metamagnetic alloys · ^{119}Sn -Mössbauer · Defects · Local strains

1 Introduction

Ni-Mn based Heusler alloys have attracted great interest during the last decades due to the multifunctional properties they exhibit, such as large magnetic-field-induced strain [1, 2],

This article is part of the Topical Collection on *Proceedings of the 4th Mediterranean Conference on the Applications of the Mössbauer Effect (MECAME 2018), Zadar, Croatia, 27-31 May 2018*
Edited by Mira Ristic and Stjepko Krehula

✉ I. Unzueta
iraultza.unzueta@ehu.es

Extended author information available on the last page of the article.

magnetoresistivity [3, 4], magnetocaloric effect [5, 6], exchange bias [7] and shape-memory effect [8]. Specifically, in the so-called metamagnetic Ni-Mn-Z ($Z = \text{In, Sn, Sb}$) shape memory alloys, the thermoelastic martensitic transformation (MT) is accompanied with a large variation of the magnetization value ΔM at the MT temperature (T_{MT}). As a result, additional multifunctional properties arise like the feasibility of a magnetic induction of the reverse MT [9] and the inverse magnetocaloric effect [10], thus enabling the development of practical applications in sensing and magnetic refrigeration. As the multifunctional properties of these alloys are directly related with the occurrence of the MT, their optimization is directly linked with the MT characteristics.

Due to magnetostructural coupling that Ni-Mn Heusler alloys exhibit, magnetic properties influence directly the MT characteristics, and vice versa. In these alloys magnetism is mainly based on the indirect exchange between Mn atoms [11]. Depending on Mn-Mn distances, the coupling may result to be ferromagnetic (FM) or anti-ferromagnetic (AF). Therefore, the magnetic properties, and as a consequence, the MT features depend strongly on composition and long-range atomic order. In fact, it has been reported [12, 13] that in some off-stoichiometric samples the exceeded Mn atoms tend to couple AF resulting on a lower macroscopic saturation magnetization M_s . Additionally, composition can be used to properly select the range of T_{MT} . Indeed, T_{MT} is very sensitive to the long-range atomic order. In Ni-Mn-In and Ni-Mn-Ga systems it is possible to shift T_{MT} by standard thermal treatments or by quenching procedures. These processes alter the atomic order, enabling shifts of T_{MT} up to $\Delta T_{\text{MT}} \approx 100 \text{ K}$ [14]. However, for Ni-Mn-Sn and Ni-Mn-Sb systems, conventional heat-treatments do not brought any variation on T_{MT} [15]. The high stability of $L2_1$ structure precludes the variation of characteristic temperatures, and the $L2_1$ -B2 transition, in essence, does not take place [15]. In such systems the long-range atomic order remains unchanged regardless heat treatments. In this regard, the modification of defects configuration and the microstructure is, along with composition, the only way to properly tune the functional properties of corresponding Ni-Mn based Heusler systems. In the case of the present study, we have focused our work in Ni-Mn-Sn systems.

Despite the aforementioned promising features, the poor mechanical properties Ni-Mn based Heusler alloys exhibit (i. e., brittleness and fragility) hinder their development towards practical applications. The cracks formed when samples are cycled through the phase transformation result in a degradation that causes samples to break [16]. As a consequence, the use of microparticles as microactuator elements is attracting increasing interest as an effective method in order to surpass the bulk limitations [17]. However, in the micro and nano scale, the microstructural state plays a key role on the MT features [18]. Indeed, the residual strain retained during the thermal cycling [16] increases the hysteresis of the MT and its irreversibility [19], and eventually degrades the MT and the shape memory effect [20]. Moreover, the presence of defects in the nanoscale may inhibit the MT and may alter FM interactions [21]. In a nutshell, although in the micro and nano regime bulk drawbacks may be effectively overcome, the control of the microstructure becomes the key point to deal with for a proper tuning of the MT.

Taking into account the magnetostructural coupling that Ni-Mn based Heusler alloys exhibit, Mössbauer spectroscopy may result a powerful tool that may shed light on the relation between the nanoscale properties and the MT features. Thereby, unlike in some previous works, in which Fe doped Ni-Mn-Sn systems are studied by ^{57}Fe Mössbauer spectroscopy [22], in the present work by means of ^{119}Sn Mössbauer spectroscopy (^{119}Sn -MS) a $\text{Ni}_{50}\text{Mn}_{35}\text{Sn}_{15}$ sample is investigated, thus ensuring the proper chemical environment of Sn atoms. Besides, the effect of the internal strain induced by milling is also evaluated by X-rays (XRD), powder neutron diffraction (PND), differential scanning calorimetry (DSC)

and magnetic measurements. The results show that, even though the milling and the post-annealing processes do not produce any variation of transition temperatures and atomic order, the induced microstructural distortions affect greatly the martensitic transformation. Additionally, the coupling between Mn atoms is altered, resulting in a significant decrease in the saturation magnetization that recovers with annealing. The obtained results confirm that, once the transition temperature has been fixed by composition, the modification of the microstructure through thermomechanical treatments appears as the best way to tune the functional properties of these alloys. Moreover, the recovery of the microstructural distortions induced by milling is directly related to the intensity of the non-magnetic component revealed by ^{119}Sn -MS.

2 Experimental

A polycrystalline $\text{Ni}_{50}\text{Mn}_{35}\text{Sn}_{15}$ alloy was synthesized from high purity elements by arc-melting furnace under argon protective atmosphere. The obtained ingot was homogenized during 24 h at 1173 K and quenched in iced water. The composition of the alloy was analyzed by EDS in a JSM-5610LV Scanning Electron Microscope (SEM). The alloy was hand milled in a Agatha mortar until a steady state revealed by ^{119}Sn -MS (≈ 20 min) was reached. The particle mean size measured by SEM was about $10\ \mu\text{m}$. The obtained powder was annealed at different temperatures: 573 K (AN573), 673 K (AN673), 773K (AN773) and 873K (AN873) for 5 minutes in order to further modify the microstructural properties. DSC measurements at a heating/cooling rate of 10 K/min were carried out in a TA Q100 calorimeter to study the magneto-structural transformations of the samples under different thermal treatments. The temperature dependence of the magnetization under different fields from 100 Oe to 60 kOe and the field dependence of the magnetization at low temperature were measured in a Quantum Design MPMS XL-7 SQUID magnetometer. Microstructural evolution was characterized by XRD measurements recorded at room temperature in a Siemens Diffractometer D5000 operating with $\text{Cu K}\alpha$ radiation and analyzed using the FullProf package programs [23]. Mössbauer spectra were obtained using a $\text{Ba}^{119\text{m}}\text{SnO}_3$ source in a transmission setup at 270 K and (ferromagnetic austenite, cubic) equipped with a triangle-wave generator at speed of 12 mm/s. Finally, the collected spectra were fitted using the NORMOS program. Finally, the atomic order was investigated by PND measurements, which were carried out at the Institute Laue-Langevin in Grenoble (France [J. López-García, J. I. Pérez-Landazábal, V. Recarte, J. A. Rodríguez-Velamazán, V. Sánchez-Alarcos, I. Unzueta, <https://doi.org/10.5291/ILL-DATA.5-24-591>]), using a D2B instrument ($\lambda = 1.59\text{Å}$).

3 Results and discussion

Figure 1 shows the temperature dependence of magnetization at 100 Oe (Fig. 1a) and 60 KOe (Fig. 1b) for both Milled and AN673 samples. As illustrated in Fig. 1, annealing does not affect neither the Curie temperature T_c nor the T_{MT} (the same behavior is observed for the rest of the AN573, AN773, and AN873 samples, not explicitly shown there). Figure 1b shows that the high-field magnetization increases in both austenite and martensite phases on annealing, but there is no variation on the transition temperatures. The only effect that annealing produces in respect to the milled sample is magnetization increase. Moreover, Fig. 1c shows the cooling-heating calorimetric measurements for the different samples,

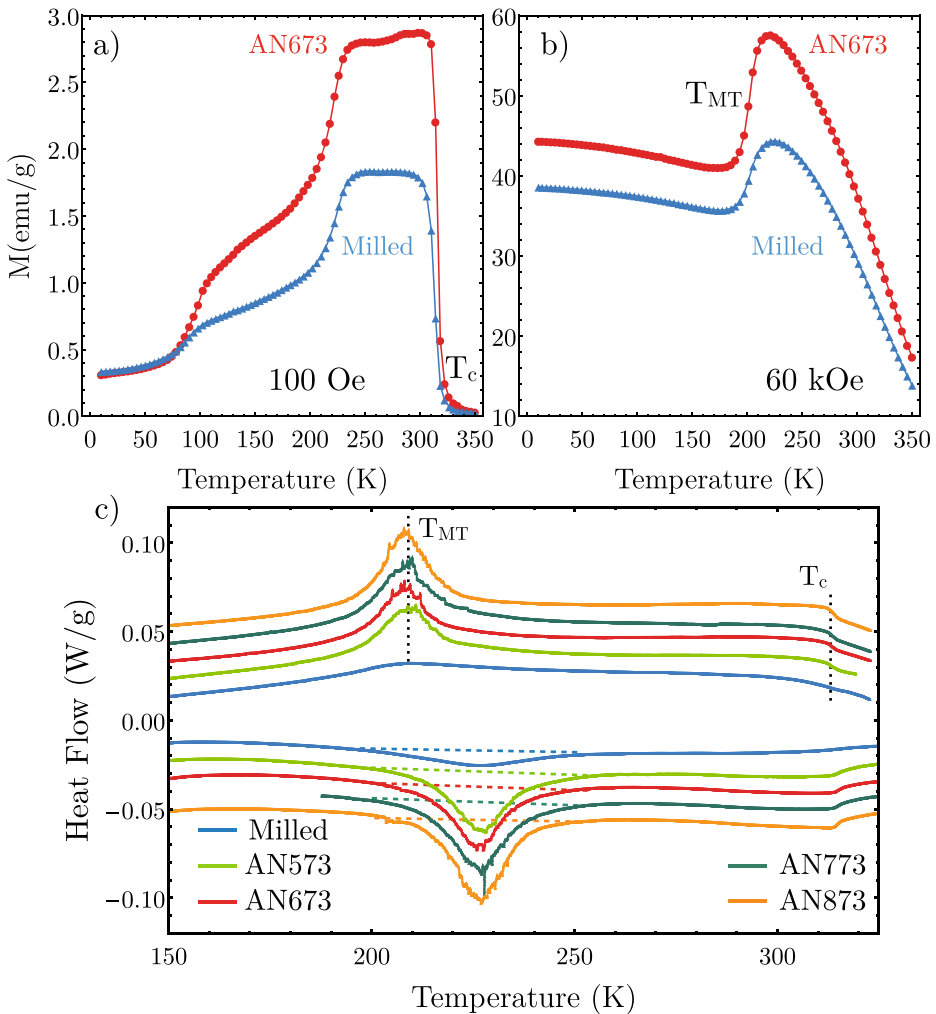


Fig. 1 Thermomagnetization curves for the Milled and AN673 samples recorded at 100 Oe **a** and 60kOe **b**. Figure **1c** DSC curves of the full series of samples (Milled and after different annealing treatments)

carried out around the T_{MT} . The exothermic and endothermic peaks observed on the cooling and heating ramps are linked to the forward (FMT) and to the reverse MT (RMT), respectively. The λ -type shoulders observed around 325 K are related to the magnetic ordering of the austenite at the T_c . The structural and magnetic transformation temperatures are summarized in Table 1, which shows that, indeed, annealing does not affect the characteristics temperatures as showed by calorimetry measurements. However, the annealing temperature increases the peak height and sharpness of the MT.

As shown in Fig. 1c and Table 1, the MT peak temperatures and the corresponding hysteresis, defined as the temperature shift between heating and cooling transformation peaks, remain unchanged for the different annealing temperatures. Likewise, the DSC measurements also indicate that the T_c of the austenite is almost unmodified by the thermal

Table 1 Temperature of DSC peaks for the FMT (M_p), for RMT (A_p), T_c , MT hysteresis and the transformation temperature interval ΔT for the set of samples

Sample	M_p (K)	A_p (K)	T_c (K)	Hys (K)	ΔT (K)
Milled	208(1)	228(1)	317(1)	19(2)	92(2)
AN573	209(1)	228(1)	322(1)	18(2)	85(2)
AN673	208(1)	226(1)	321(1)	18(2)	83(2)
AN773	209(1)	227(1)	322(1)	19(2)	75(2)
AN873	208(1)	227(1)	322(1)	20(2)	70(2)

treatments. On the other hand, the temperature range where the transformation spreads, ΔT , becomes gradually reduced diminishing from 90 K to 70 K (see Table 1). Such transformation interval has been determined by the average value of the difference between the starting and finishing transformation temperatures for the FMT (M_s and M_f , respectively) and for the RMT (temperatures A_s and A_f , respectively). Thus, although the temperatures of the magnetostructural transitions, T_{MT} and T_c , do not change with the post-milling, the reduction of ΔT indicates that the dynamics of the transformation is strongly affected by the microstructural evolution taking place during the heat treatments. The effect of annealing on the studied sample is an increase of the saturation magnetization and a narrowing of the calorimetric MT peaks. Taking into account that both T_c and the MT temperature are highly sensitive to atomic order [24], the lack of variation in these transition temperatures seems to indicate a null effect of annealing on the atomic order [15].

In order to correlate the microstructure with the annealing treatments, XRD measurements have been carried out in austenitic phase at room temperature. Figure 2 shows the XRD patterns obtained for the different samples. All of them display the characteristic [220], [400] and [422] peaks corresponding to the well-known Heusler $L2_1$ cubic structure, ($Fm\bar{3}m$) space group [15]. The reflection peaks lie at the same angles in all cases, indicating an almost null change of cell parameter (see the cell parameter values in the upper right corner of each diffraction pattern in Fig. 2). Nevertheless, the peaks become narrower as the annealing temperature increases, which, as expected, suggests a variation on the microstructural parameters. Figure 3a displays the evolution of internal strains and grain size determined from the Le Bail analysis of the diffraction patterns along the series of samples. The internal strains decrease and the grain size increases with the increasing annealing temperature, evolving from small grain size with high percentage of strain ($88.98 \pm 0.02 \text{ \AA}$ and $9.32 \pm 0.03 \%$, respectively, on the Milled sample) to bigger grains and lower strains ($222.08 \pm 0.06 \text{ \AA}$ and $1.09 \pm 0.03 \%$, respectively, in AN873).

Once determined the internal strains, we can depict the MT and magnetic properties as a function of the microstructural evolution. Figure 3b shows the MT temperature range as a function of internal strains. It can be seen that ΔT increases almost linearly with the microstrains, in agreement with an increase of the elastic energy, indicating that ΔT variation is directly related to microstructural changes. The long-range atomic order and magnetic ordering of the austenite were analyzed from Powder Neutron Diffraction (PND) measurements. Figure 4 shows the experimental and fitted PND patterns obtained from the milled and AN673 samples at 270 K (ferromagnetic austenite). Both samples show the cubic $L2_1$ structure with the same lattice parameter ($6.004(1) \text{ \AA}$ for the Milled sample and $6.003(1) \text{ \AA}$ for the AN673 sample) compatible with the calculated values by X-rays (see Fig. 2). The magnetic and structural parameters for 4a and 4b Wyckoff positions obtained after Rietveld

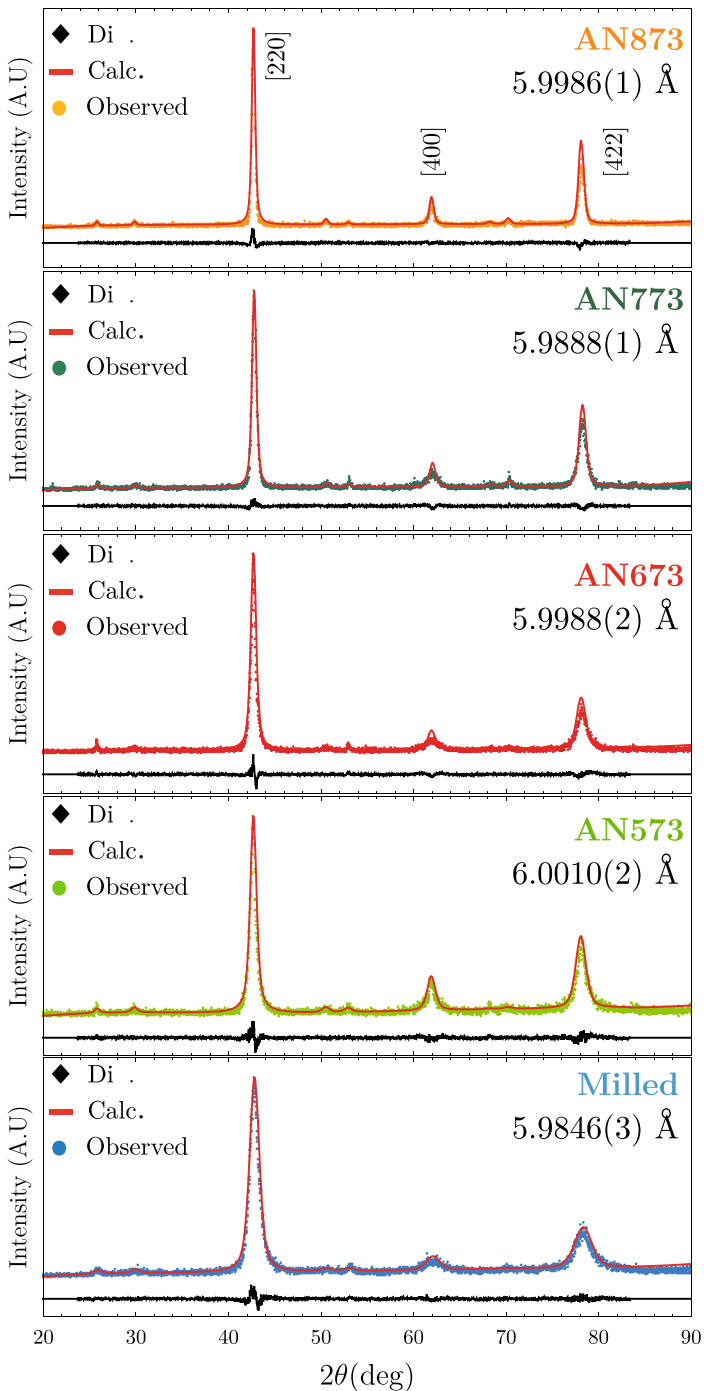


Fig. 2 a) Room temperature XRD patterns and the corresponding calculated lattice parameters for Milled, AN573, AN673, AN773 and AN873 samples. The dots are the observations, the red line the calculated pattern and the black line the difference between observed and calculated intensity

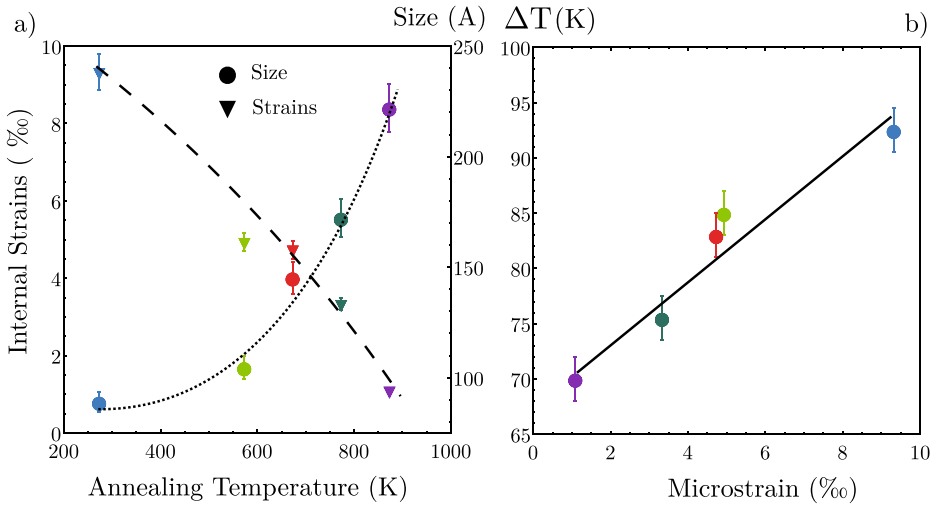


Fig. 3 **a** Evolution of grain size and strain as a function of annealing temperature. **b** Martensitic transformation temperature interval ΔT as a function of internal strains

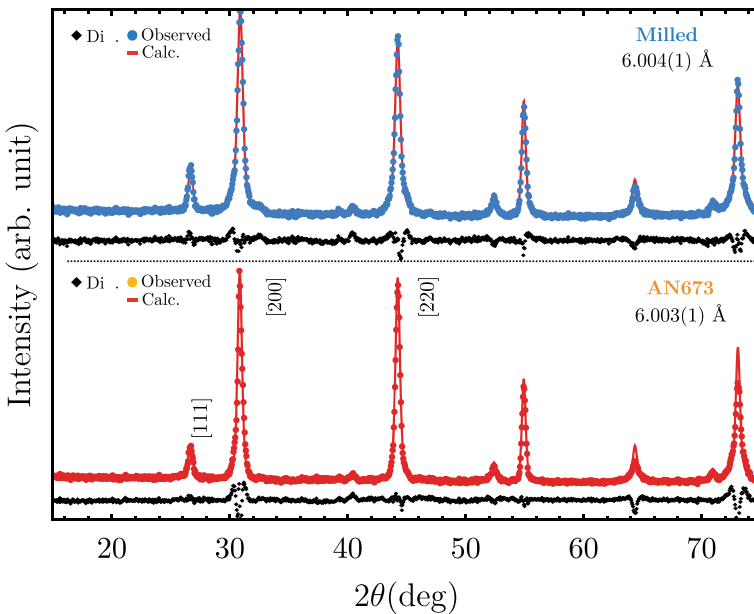
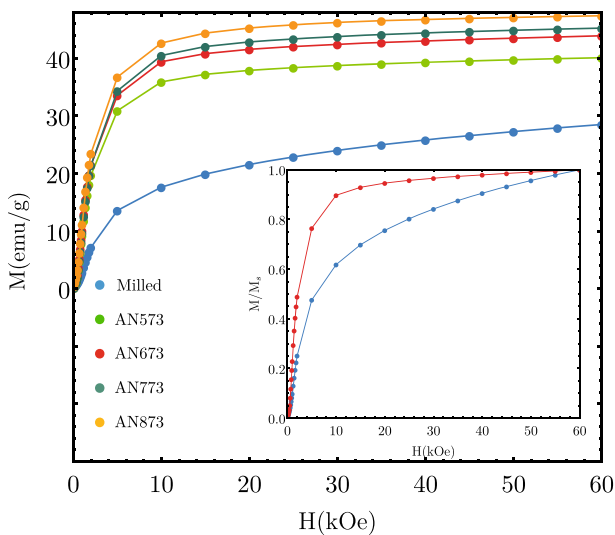


Fig. 4 Rietveld refinement of the neutron diffraction patterns for the Milled (top) and AN673 (bottom) samples recorded at 270 K

refinement are shown in Table 2. The occupancies are almost the same in both cases ($4a$ positions are mainly occupied by Mn atoms and $4b$ positions are occupied by both Mn and Sn atoms [12], which means that the degree of $L2_1$ atomic order is the same in both samples.

Table 2 Occupancy and μ magnetic moment values obtained from the Rietveld refinement for 4*a* and 4*b* positions for the Milled and AN673 samples. The occupancy of Ni position has been fixed to be 1.

	Site 4 <i>a</i>		Site 4 <i>b</i>	
	Occupancy	$\mu(\mu_B)$	Occupancy	$\mu(\mu_B)$
Milled	Mn 0.95(4)	1.26(6)	Mn 0.41(4)	-0.45(6)
	Ni 0.05(4)		Ni 0.02(0)	
	Sn (—)		Sn 0.57(4)	
AN673	Mn 0.94(3)	2.58(2)	Mn 0.43(3)	0.37(2)
	Ni 0.06(3)		Ni 0.05(0)	
	Sn (—)		Sn 0.52(3)	

**Fig. 5** Magnetic field dependence of magnetization of the set of samples recorded at 10 K, martensite. The inset shows the normalized M/M_s of the Milled and the AN873 sample for a better visualization of their different approach towards saturation

Therefore, in agreement with the observed absence of variation in the transition temperatures, no atomic order variation is brought by annealing. Nevertheless, interestingly, the magnetic coupling between Mn atoms in 4*a* and 4*b* positions drastically evolves from AF to FM upon annealing, in spite of neither atomic order nor lattice parameter do change. It is worth noting, that in agreement with XRD, the reflection peaks are clearly broader in the Milled sample. This points out a microstructural evolution (higher crystallite size or lower microstrains in the annealed sample), which could be behind the magnetic one.

Magnetic measurements at low temperature were carried out in order to determine the evolution of magnetic properties of the martensite during the microstructural recovery induced by the thermal treatments. Figure 5 shows the magnetic field dependence of the magnetization of the different samples at 10 K. It is worth noting the increase of the saturation magnetization, as well as the clear change of the shape of the curve, with the increasing annealing temperatures. Additionally, the inset of Fig. 5 shows the normalized $M(H)$ cycle

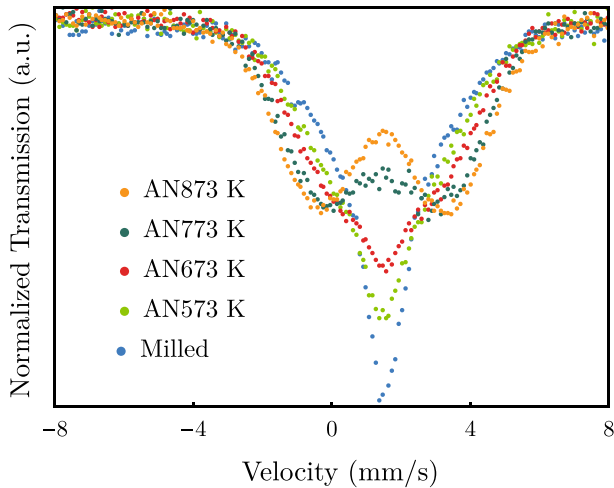


Fig. 6 Experimental ^{119}Sn -MS spectra measured for all the studied samples

of Milled and AN673 samples recorded at 10 K, where different approach to saturation is clearly observed. This different approach to saturation and the increase of the saturation magnetization on annealing can be ascribed to a different AF contribution to the magnetic moment between the Milled and AN673 samples, as indicated by the PND results shown in Table 2.

Summarizing, in contrast to the behavior reported in Ni-Mn-Ga and Ni-Mn-In by Sánchez-Alarcos et al. in Ref. [25], calorimetric, XRD and PND measurements and magnetic characterization performed in $\text{Ni}_{50}\text{Mn}_{35}\text{Sn}_{15}$ show clearly the null effect of annealing on long-range atomic order, however, such measurements indicate a noticeable microstructural variation with annealing. It is known that in Heusler alloys, cold working on bulk alloys induces the presence of anti-phase boundaries (APB) surrounded by dislocations (dislocations in atomic ordered structures appear as super-dislocations; a pair of dislocations separated by an APB where the atomic order, and consequently the ferromagnetic coupling, is modified) [26, 27]. Therefore, it is expected that the presence of APBs causes the internal strain observed in the Milled samples in XRD and PND measurements.

The reduction of the density of APBs with annealing, as a result of the annihilation of dislocations [28], will be the cause of the observed reduction of the internal strain of the annealed samples, and so, of the narrowing of DSC's MT's peaks. The Rietveld refinements of PND patterns (see Table 2) indicate the presence of AF coupling between Mn atoms in the Milled sample that after annealing become mostly FM coupled. Moreover, interatomic distances vary slightly at APBs [29], and taking into account that the magnetic coupling is very dependent on Mn-Mn interatomic distance [30], PND results suggest that APBs (present in milled samples) may be the cause of the AF coupling observed. Indeed, the exchange interaction between the second nearest neighbor Mn atoms located across the APB can become AF in an otherwise FM material [31, 32].

In order to ascertain the nature of the effect of annealing on the magnetic properties, the magnetism was studied at the atomic level by ^{119}Sn -MS. Figure 6 shows the experimental ^{119}Sn -MS spectra of all the studied samples. The spectrum of the Milled sample is mainly composed of a singlet; however, in the case of AN573 the depth of the singlet decreases

Fig. 7 Fitted ^{119}Sn -MS spectra measured for all the studied samples

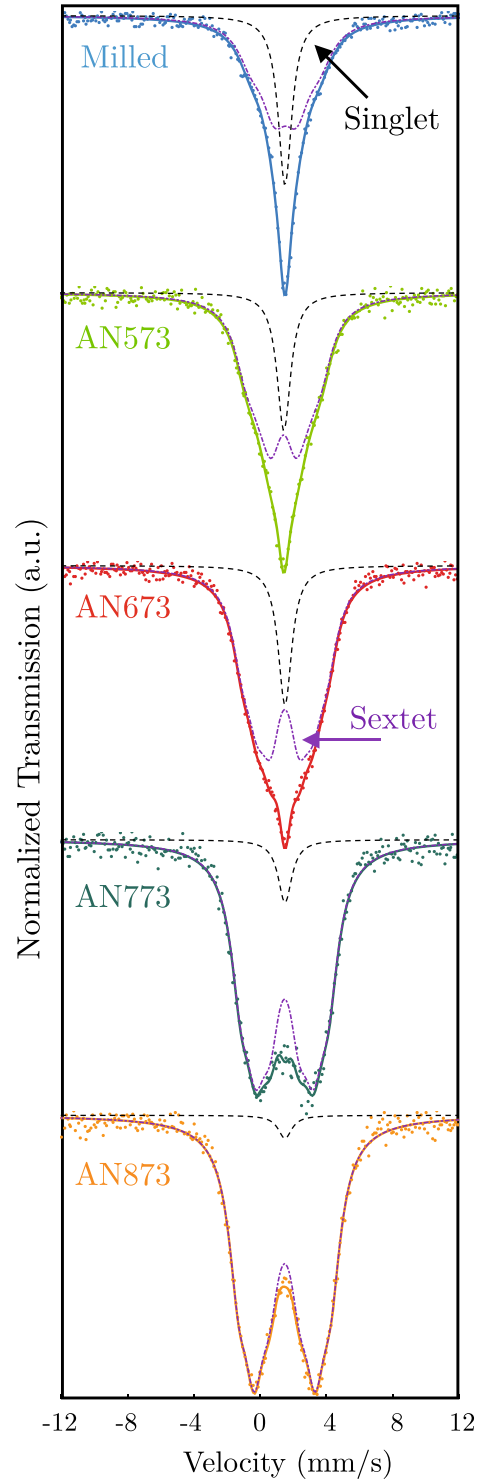


Table 3 Hyperfine parameters obtained from the fitting procedure of all the studied samples. B_{hf} hyperfine field of the sextet component and the A_s intensity of the singlet component, along with δ isomer shift and Γ line-width parameters. δ and Γ have been constrained to be the same for both subspectra

Sample	B_{hf} (T)	A_s (%)	δ (mm/s)	Γ (mm/s)
Milled	4.1(1)	%31(3)	1.53(1)	1.96(1)
AN573	4.6(2)	%18(1)	1.48(1)	1.67(7)
AN673	5.2(1)	%15(1)	1.48(1)	1.54(5)
AN773	5.3(1)	%6(1)	1.48(1)	1.51(4)
AN873	5.6(1)	%1(1)	1.48(1)	1.50(2)

and at higher annealing temperatures a clear broadening of the spectra appears. Indeed, in the case of AN873 sample a magnetic contribution is observed. Sn atoms do not carry any intrinsic magnetic moment, but a transferred hyperfine field can be induced from neighbor magnetic Mn atoms [33].

Figure 7 shows the fitting of the previously cited spectra. All the spectra have been fitted using two discrete contributions: a non-magnetic singlet and a magnetic subspectrum. Although in the case of AN873 sample the spectrum can be also be fitted with a single sextet component, better χ^2 values are systematically obtained by considering also the singlet contribution. Taking into account the cubic structure of the sample (austenite phase with $L2_1$ structure) the quadrupole shift has been taken to be zero. It is worth noting, that in the fitting procedure the line-width and the isomer shift of the two subspectra have been constrained to be the same. Table 3 shows the results of the fitting procedure. Similar values of the δ isomer shift were obtained for all the samples, indicating that the chemical order in the surrounding of Sn atoms remains the same, independently of the annealing process [34]. However, the line-width parameter Γ listed in Table 3 decreases as the annealing temperature increases. The Γ parameter is sensitive to slight distortions of the local environment of the Mössbauer probe atoms [35], so its decrease indicates a microstructural evolution on the very close environment of Sn atoms.

The relative intensities of both Mössbauer contributions change gradually with the annealing temperature, being the magnetic subspectrum practically the only one dominating the AN873 spectrum. The main common feature is the decrease in the singlet component (A_s) and increase in the B_{hf} magnetic hyperfine field value, with increasing annealing temperature, indicating that the number of Sn atoms with transferred hyperfine field increases with annealing. The major recovery of the Γ parameter occurs in the first two annealing at 573 K and 673 K. The dislocation annihilation at these temperatures has been previously reported in other Heusler alloys [27, 36]. However, as the ^{119}Sn -MS shows (see the evolution of the A_s in Table 3) the recovery process continues above 673 K without a significant change in Γ parameter. In this region, the recovery would be mediated by the elimination of point defects, such as vacancies [37], introduced during the milling of the sample. Figure 8a shows the width of the temperature range in which the MT is extended, ΔT , as a function of the singlet contribution A_s , and Fig. 8b, shows the singlet contribution A_s of the ^{119}Sn -MS versus the internal strains. Taking into account these two figures and Fig. 3b, they clearly indicate that the non-magnetic singlet contribution is directly related to the internal strain-state and the distorted regions present in the sample. Therefore, the influence of the microstructural recovery on the MT can be directly tracked by the singlet component revealed by ^{119}Sn -MS.

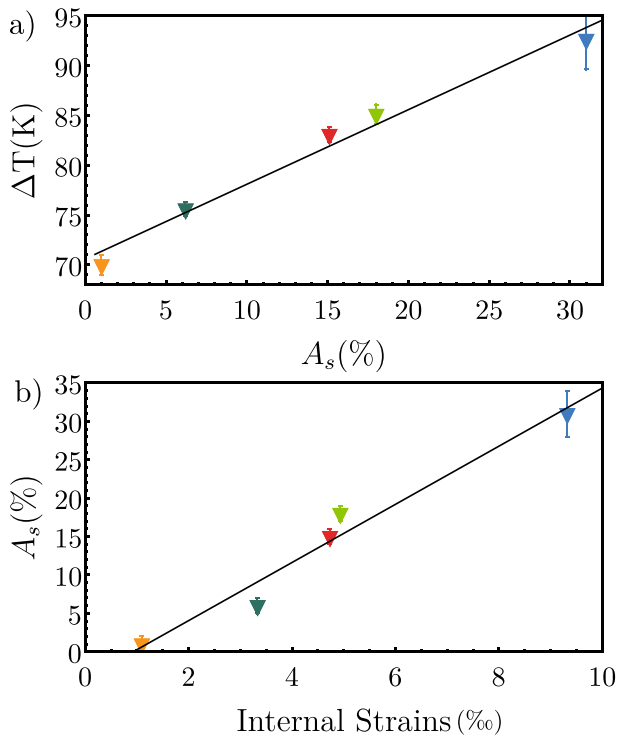


Fig. 8 a Evolution of ΔT vs A_s . b Direct dependence of A_s and Internal strains

4 Conclusions

The effect of combined mechanical and thermal treatments in the $\text{Ni}_{50}\text{Mn}_{35}\text{Sn}_{15}$ metamagnetic shape memory alloy was studied by XRD, PND, DSC, magnetometry and ^{119}Sn -MS. A hand-milled alloy has been annealed at different temperatures producing different microstructural states that are correlated with the magneto-structural properties. Milling induces a high average of internal strain and, as consequence, a small grain size and a high density of defects. Annealing relaxes the internal strain, increasing the grain size, recovering the MT and enhancing the magnetostructural properties. Upon annealing, the density of non-magnetic defects and their strain field decrease, thus leading to an increase of the saturation magnetization and a decrease of the martensitic transformation temperature range, respectively. It has been shown that both, MT and magnetic properties of $\text{Ni}_{50}\text{Mn}_{35}\text{Sn}_{15}$ are very sensitive to slight microstructural distortions even without inducing any change in atomic order. Due to the high stability that the Ni-Mn-Sn systems show against the atomic disorder, this result opens an additional way to properly tune the multifunctional properties in the Ni-Mn-Sn systems. From a technological point of view, once the transition temperature has been fixed by the composition, the characteristics and therefore the properties linked to the martensitic transformation can be modified by thermomechanical treatments. Finally, we show that ^{119}Sn -MS is a proper technique to link the MT with the microstructural state, becoming a practical tool to assess the microstructural characterization of the local strains and defect state in order to properly tune the MT towards future applications.


Acknowledgments This work has been supported by Spanish Ministry of Economy and Competitiveness under MAT2015-65165-C2-R (MINECO / FEDER) project, and by Basque Government Grant No. IT-1005-16. I. Unzueta also wants to acknowledge financial support from the Basque Government Grant No. PRE2014-1-214. J. López-García acknowledges ILL for his Ph.D. contract. We would like to thank also ILL and SpINS for beam time allocation.

References

- Ullakko, K., Huang, J.K., Kantner, C., O'Handley, R.C., Kokorin, V.V.: Appl. Phys. Lett. **69**(13), 1966 (1996). <https://doi.org/10.1063/1.117637>
- Chmielus, M., Zhang, X.X., Witherspoon, C., Dunand, D.C., Müllner, P.: Nat. Mater. **8**, 863 EP (2009). <https://doi.org/10.1038/nmat2527>
- Yu, S.-Y., Liu, Z.H., Liu, G.D., Chen, J.L., Cao, Z.X., Wu, G.H., Zhang, B., Zhang, X.X.: Appl. Phys. Lett. **89**(16), 162503 (2006). <https://doi.org/10.1063/1.2362581>
- Ito, W., Ito, K., Umetsu, R.Y., Kainuma, R., Koyama, K., Watanabe, K., Fujita, A., Oikawa, K., Ishida, K., Kanomata, T.: Appl. Phys. Lett. **92**(2), 021908 (2008). <https://doi.org/10.1063/1.2833699>
- Krenke, T., Duman, E., Acet, M., Wassermann, E.F., Moya, X., Mañosa, L., Planes, A.: Nat. Mater. **4**, 450 EP (2005). <https://doi.org/10.1038/nmat1395>
- Mañosa, L., González-Alonso, D., Planes, A., Bonnot, E., Barrio, M., Tamarit, J.L., Aksoy, S., Acet, M.: Nat. Mater. **9**, 478 EP (2010). <https://doi.org/10.1038/nmat2731>
- Khan, M., Dubenko, I., Stadler, S., Ali, N.: Appl. Phys. Lett. **91**(7), 072510 (2007). <https://doi.org/10.1063/1.2772233>
- Sutou, Y., Imano, Y., Koeda, N., Omori, T., Kainuma, R., Ishida, K., Oikawa, K.: Appl. Phys. Lett. **85**(19), 4358 (2004). <https://doi.org/10.1063/1.1808879>
- Kainuma, R., Imano, Y., Ito, W., Sutou, Y., Morito, H., Okamoto, S., Kitakami, O., Oikawa, K., Fujita, A., Kanomata, T., Ishida, K.: Nature **439**, 957 EP (2006). <https://doi.org/10.1038/nature04493>
- Moya, X., Mañosa, L., Planes, A., Aksoy, S., Acet, M., Wassermann, E.F., Krenke, T.: Phys. Rev. B **75**, 184412 (2007). <https://doi.org/10.1103/PhysRevB.75.184412>
- Şaşoğlu, E., Sandratskii, L.M., Bruno, P.: Phys. Rev. B **77**, 064417 (2008). <https://doi.org/10.1103/PhysRevB.77.064417>
- Krenke, T., Acet, M., Wassermann, E.F., Moya, X., Mañosa, L., Planes, A.: Phys. Rev. B **72**, 014412 (2005). <https://doi.org/10.1103/PhysRevB.72.014412>
- Ma, L., Wang, W.H., Lu, J.B., Li, J.Q., Zhen, C.M., Hou, D.L., Wu, G.H.: Appl. Phys. Lett. **99**(18), 182507 (2011). <https://doi.org/10.1063/1.3651767>
- Recarte, V., Pérez-Landazábal, J., Sánchez-Alarcos, V., Rodríguez-Velamazán, J.: Acta Mater. **60**(5), 1937 (2012). <https://doi.org/10.1016/j.actamat.2012.01.020>. <http://www.sciencedirect.com/science/article/pii/S1359645412000584>
- Sánchez-Alarcos, V., Pérez-Landazábal, J., Recarte, V., Lucia, I., Vélez, J., Rodríguez-Velamazán, J.: Acta Mater. **61**(12), 4676 (2013). <https://doi.org/10.1016/j.actamat.2013.04.040>. <http://www.sciencedirect.com/science/article/pii/S1359645413003133>
- Schergell, H., Kneissl, A.: Acta Mater. **50**(2), 327 (2002). [https://doi.org/10.1016/S1359-6454\(01\)00342-1](https://doi.org/10.1016/S1359-6454(01)00342-1). <http://www.sciencedirect.com/science/article/pii/S1359645401003421>
- Kumar, S.V., Singh, R., Raja, M.M., Kumar, A., Bysakh, S., Mahendran, M.: Intermetallics **71**, 57 (2016). <https://doi.org/10.1016/j.intermet.2015.12.012>. <http://www.sciencedirect.com/science/article/pii/S096679515301126>
- Peruman, K.V., Vinodh Kumar, S., Pushpanathan, K., Mahendran, M.: Funct. Mater. Lett. **4**(4), 415 (2011). <https://doi.org/10.1142/S1793604711002329>
- Prasanna, A.A., Ram, S.: Sci. Technol. Adv. Mater. **14**(1), 015004 (2013). <https://doi.org/10.1088/1468-6996/14/1/015004>. PMID: 27877562
- Rao, G., Wang, J., Han, E., Ke, W.: Mater. Lett. **60**(6), 779 (2006). <https://doi.org/10.1016/j.matlet.2005.10.023>. <http://www.sciencedirect.com/science/article/pii/S0167577X05009766>
- Alves, A.L., Passamani, E.C., Nascimento, V.P., Takeuchi, A.Y., Larica, C.: J. Phys. D: Appl. Phys. **43**(34), 345001 (2010). <http://stacks.iop.org/0022-3727/43/i=34/a=345001>
- Umetsu, R.Y., Kainuma, R., Amako, Y., Taniguchi, Y., Kanomata, T., Fukushima, K., Fujita, A., Oikawa, K., Ishida, K.: Appl. Phys. Lett. **93**(4), 042509 (2008). <https://doi.org/10.1063/1.2960551>
- Rodríguez-Carvajal, J.: Physica B **192**(1), 55 (1993). [https://doi.org/10.1016/0921-4526\(93\)90108-I](https://doi.org/10.1016/0921-4526(93)90108-I). <http://www.sciencedirect.com/science/article/pii/0921452693901081>

24. Sokolovskiy, V.V., Buchelnikov, V.D., Zagrebin, M.A., Entel, P., Sahoo, S., Ogura, M.: *Phys. Rev. B* **86**, 134418 (2012). <https://doi.org/10.1103/PhysRevB.86.134418>
25. Sánchez-Alarcos, V., Recarte, V., Pérez-Landazábal, J., Gómez-Polo, C., Rodríguez-Velamazán, J.: *Acta Mater.* **60**(2), 459 (2012). <https://doi.org/10.1016/j.actamat.2011.10.026>. <http://www.sciencedirect.com/science/article/pii/S1359645411007312>
26. Ikeda, K., Takahashi, S.: *Phys. Rev. B* **30**, 3808 (1984). <https://doi.org/10.1103/PhysRevB.30.3808>
27. Takahashi, S., Shinohara, T.: *J. Phys. F: Met. Phys.* **12**(12), 3115 (1982). <http://stacks.iop.org/0305-4608/12/i=12/a=037>
28. Unzueta, I., López-García, J., Sánchez-Alarcos, V., Recarte, V., Pérez-Landazábal, J.I., Rodríguez-Velamazán, J.A., Garitaonandia, J.S., García, J.A., Plazaola, F.: *Appl. Phys. Lett.* **110**(18), 181908 (2017). <https://doi.org/10.1063/1.4982630>
29. Niitsu, K., Minakuchi, K., Xu, X., Nagasako, M., Ohnuma, I., Tanigaki, T., Murakami, Y., Shindo, D., Kainuma, R.: *Acta Mater.* **122**, 166 (2017). <https://doi.org/10.1016/j.actamat.2016.09.035>. <http://www.sciencedirect.com/science/article/pii/S1359645416307340>
30. Lázpita, P., Barandiarán, J.M., Gutiérrez, J., Feuchtwanger, J., Chernenko, V.A., Richard, M.L.: *J. Phys.* **13**(3), 033039 (2011). <http://stacks.iop.org/1367-2630/13/i=3/a=033039>
31. Young, A.P., Jakubovics, J.P.: *J. Phys. F: Met. Phys.* **5**(10), 1866 (1975). <http://stacks.iop.org/0305-4608/5/i=10/a=010>
32. Kamiyama, T., Shinohara, T., Tomiyoshi, S., Minonishi, Y., Yamamoto, H., Asano, H., Watanabe, N.: *J. Appl. Phys.* **68**(9), 4741 (1990). <https://doi.org/10.1063/1.346128>
33. Michael Kalvius, P.K.: *The Rudolf Mössbauer Story*. Springer-Verlag, Berlin (2012)
34. Kistner, O.C., Sunyar, A.W.: *Phys. Rev. Lett.* **4**, 412 (1960). <https://doi.org/10.1103/PhysRevLett.4.412>
35. Dominic, F.J.B., Dickson, P.E.: *Mössbauer Spectroscopy*. Cambridge University Press, Berlin (1986)
36. Schaf, J., Dang, K.L., Veillet, P., Campbell, I.A.: *J. Phys. F: Met. Phys.* **13**(6), 1311 (1983). <http://stacks.iop.org/0305-4608/13/i=6/a=028>
37. Merida, D., García, J.A., Sánchez-Alarcos, V., Pérez-Landazábal, J.I., Recarte, V., Plazaola, F.: *Appl. Phys. Lett.* **104**(23), 231905 (2014). <https://doi.org/10.1063/1.4882903>

Affiliations

I. Unzueta^{1,3}  · **J. López-García**² · **V. Sánchez-Alarcos**^{5,6} ·
V. Recarte^{5,6} · **J. I. Pérez-Landazábal**^{5,6} ·
J. A. Rodríguez-Velamazán² · **J. S. Garitaonandia**^{3,4} ·
J. A. García^{3,4} · **F. Plazaola**¹

J. López-García
lopez-garcia@ill.fr

V. Sánchez-Alarcos
vicente.sanchez@unavarra.es

V. Recarte
recarte@unavarra.es

J. I. Pérez-Landazábal
ipzlanda@unavarra.es

J. A. Rodríguez-Velamazán
velamazan@ill.fr

J. S. Garitaonandia
js.garitaonandia@ehu.eus

J. A. García
joseangel.garcia@ehu.eus

F. Plazaola
fernando.plazaola@ehu.eus

¹ Department of Electricity and Electronics, University of the Basque Country UPV/EHU, 48940, Leioa, Spain

² Institut Laue-Langevin, 71 Avenue des Martyrs, 38000 Grenoble, France

³ BCMaterials, University of the Basque Country UPV/EHU, 48940, Leioa, Spain

⁴ Department of Applied Physics II, University of the Basque Country UPV/EHU, 48940, Leioa, Spain

⁵ Department of Science, Universidad Pública de Navarra, Campus de Arrosadia, 31006 Pamplona, Spain

⁶ Institute for Advanced Materials (INAMAT), Universidad Pública de Navarra, Campus de Arrosadia, 31006 Pamplona, Spain